

The Different Relationships between the ENSO Spring Persistence Barrier and Predictability Barrier

YISHUAI JIN,^{a,b} ZHENGYU LIU,^c AND WANSUO DUAN^d

^a Key Laboratory of Physical Oceanography, Ministry of Education, Ocean University of China, Qingdao, China

^b Open studio for Ocean-Climate-Isotope Modeling, Pilot National Laboratory for Marine Science and Technology (Qingdao), Qingdao, China

^c Atmospheric Science Program, Department of Geography, The Ohio State University, Columbus, Ohio

^d State Key Laboratory of Numerical Modeling for Atmospheric Sciences and Geophysical Fluid Dynamics (LASG), Institute of Atmospheric Physics, Chinese Academy of Sciences, Beijing, China

(Manuscript received 7 January 2021, in final form 23 May 2022)

ABSTRACT: In this paper, we investigate the relationship between the El Niño–Southern Oscillation (ENSO) spring persistence barrier (PB) and predictability barrier (PD) and apply it to explain the interdecadal modulation of ENSO prediction skill using the anomaly correlation coefficient (ACC). Previous studies showed that a longer persistence (i.e., autocorrelation) tends to produce a higher prediction skill. Using the recharge oscillator model of ENSO, both analytical and numerical solutions suggest that the predictability (i.e., ACC) is related to the persistence of sea surface temperature (SST) and cross correlation between SST and subsurface ocean heat content in the tropical Pacific. In particular, a larger damping rate in SST anomalies will lead to a lower persistence and ACC and a stronger PD. However, a shortened ENSO period, which controls the cross correlation, will lead to a lower persistence but a higher ACC associated with a weaker PD. Finally, we apply our solutions to observations and suggest that a higher ACC associated with a weaker PD after 1960 is caused by the shortened ENSO period.

KEYWORDS: ENSO; Persistence; Prediction skill; ENSO period

1. Introduction

The El Niño–Southern Oscillation (ENSO) phenomenon is the most prominent interannual signal of the climate system (McPhaden et al. 2006; Cai et al. 2018), influencing patterns of weather variability worldwide. As such, its predictability and prediction have received considerable attention with one major problem being the boreal spring persistence barrier (PB) and the associated spring predictability barrier (PD). Spring PB is derived from the time series of anomalous tropical Pacific sea surface temperature (SST) (e.g., Niño-3.4; 5°S–5°N, 170°–120°W; McPhaden 2003; Ren et al. 2016), sea level pressure (Troup 1965; Webster and Yang 1992), and rainfall (Walker and Bliss 1932; Wright 1979). Regardless of the initial month, a damped persistence forecast loses its predictability most rapidly in the following April–June, forming the spring PB of ENSO (Jin et al. 2020). Spring PD, on the other hand, indicates the dramatic drop of prediction skill in the spring in the numerical ENSO predictions. Overall, the spring PB indicates a drop of persistence (indicated by the lagged autocorrelation) in the spring while spring PD shows a significant loss of prediction skill (calculated by the ensemble forecasts against the observation of ENSO) in the spring. They two are related but not identical (Jin et al. 2021).

Many studies have shown that a longer persistence of SST anomaly, as indicated by autocorrelation, in the observation tends to have a higher prediction skill, such that a stronger PB tends to lead to a stronger PD (Jin et al. 2021). By using a simple statistical model and a fully coupled general circulation model, Jin et al. (2018) found a persistence–skill rule: a larger SST persistence tends to produce a higher forecast skill. Wang et al. (2021) demonstrated that a stronger PB is accompanied with a stronger PD through the Lorenz ‘63 model (Lorenz 1963). This opinion can also be pointed out in Fig. 1a using the simple recharge oscillator model (ROM). When persistence is higher (black dashed line vs red dashed line) because of the weaker damping system, the anomaly correlation coefficient (ACC; hereafter we use ACC to represent predictability) is larger (black solid line vs red solid line; more details about the experiments can be seen in section 3).

As ENSO is not a purely damping system, its predictability comes both from SST persistence and elsewhere (e.g., subsurface or wind stress in the equatorial Pacific; Meinen and McPhaden 2000; Anderson 2007). For instance, in the recharge oscillator framework of ENSO, the slow evolution of upper-ocean heat content (OHC) in the tropical Pacific can be a very important factor for ENSO forecasting (McPhaden 2003; Jin et al. 2021). When ENSO persistence is lower, the subsurface OHC can be an indicator such that the predictability of ENSO may be higher. This point can be further identified in Fig. 1b. When the ENSO period is shorter, persistence of the SST is lower (red dashed line vs black dashed line) while ACC is higher (red solid line vs black solid line). This can be understood physically. As ENSO is a well-known oscillation, the lagged autocorrelation of ENSO SST exhibits a clear cycle,

 Denotes content that is immediately available upon publication as open access.

Corresponding author: Yishuai Jin, jinyishuai@126.com

DOI: 10.1175/JCLI-D-22-0013.1

© 2022 American Meteorological Society. For information regarding reuse of this content and general copyright information, consult the AMS Copyright Policy (www.ametsoc.org/PUBSReuseLicenses).

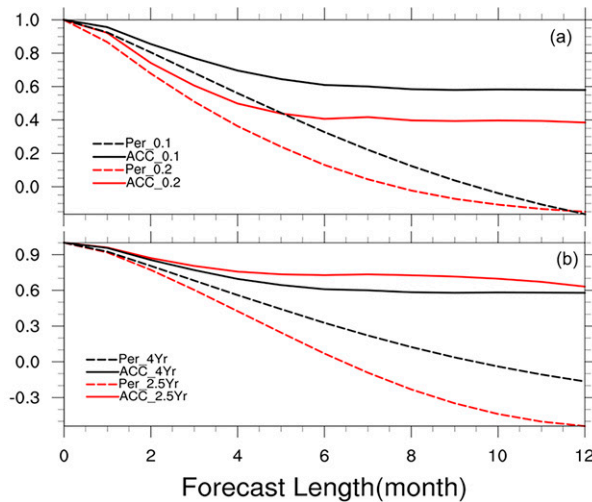


FIG. 1. The persistence (calculated by the lagged autocorrelation; dashed lines; hereafter we use “Per” to represent persistence in the legend) and ACC (solid lines) under different damping rates (λ) and ENSO periods (ω_0) through the numerical solution of recharge oscillator model [Eqs. (2.1) and (2.2)]. Results are shown (a) when λ decreases from 0.2 month^{-1} (red) to 0.1 month^{-1} (black) and the ENSO period is 4 years, and (b) when ENSO period ranges from 4 years (black) to 2.5 years (red) and $\lambda = 0.1 \text{ month}^{-1}$.

namely a drop of lagged autocorrelation at the first half cycle and an increase at the second half cycle. When the ENSO period is shortened, the drop of lagged autocorrelation of ENSO SST can be more intense at the first half cycle (i.e., less persistence; Jin and Liu 2021). On the other hand, this shortened period is caused by a stronger thermocline feedback (Jin 1997). A stronger signal from the subsurface can provide an additional information for prediction as the subsurface of tropical Pacific is a predictor for ENSO events (McPhaden 2003). Therefore, the predictability of ENSO is not actually low.

To our knowledge, the relationship between ENSO spring PB and PD is still unclear. As mentioned above, a lower persistence can be accompanied with a higher ENSO predictability, which also shows that a stronger spring PB may not be able to indicate a stronger spring PD. As such, in this paper, we want to answer the following two questions: 1) What is the relationship between persistence and prediction skill theoretically and numerically in ENSO (more specifically, the relationship between ENSO spring PB and PD)? 2) Can this relationship be applied to explain the interdecadal modulation of ENSO predictability in the real world?

In this paper, we attempt to understand the relationship between spring PB and PD in the context of the recharge oscillator and apply it to explain the interdecadal modulation of ENSO prediction skill in the real world. Both analytical and numerical solutions of ACC are derived in the framework of the recharge oscillator. These solutions show that both persistence and ENSO period contribute to ACC. In particular, a stronger damping causes a lower persistence and ACC, leading to a stronger spring PB and PD, while a shortened ENSO

period leads to a lower persistence and a higher ACC, which corresponds to a stronger spring PB and a weaker spring PD. Finally, we show that a smaller ACC associated with a stronger spring PD before 1960 is caused by the lengthened ENSO period.

The paper is arranged as follows. The recharge oscillator model, the second-order autoregression model, the verification measures of ACC, and the reanalysis data we use are presented in section 2. In section 3, we explore the relationship between persistence and predictability both analytically and numerically. Further study about spring PB and PD is identified in section 4. In section 5, we interpret the interdecadal modulation of ENSO predictability in the light of these modeled relationships. A summary and discussion are given in section 6.

2. Model, method, and data

a. The recharge oscillator model

Our ENSO model is based upon the recharge oscillator framework of ENSO (Jin 1997), which describes the relationship between variations in OHC and SST anomalies (Meinen and McPhaden 2000). This recharge oscillator model captures the dynamic relationship between the equatorial Pacific thermocline (or OHC) anomaly (H) and eastern equatorial Pacific SST anomaly (T) and can be written as follows (Burgers et al. 2005):

$$\frac{dT}{dt} = -\lambda T + \omega_0 H + \xi, \quad (2.1)$$

$$\frac{dH}{dt} = -\omega_0 T. \quad (2.2)$$

Here, λ is the damping rate (or $-\lambda$ the growth rate) of the SST anomaly, the ENSO linear frequency is ω_0 , ξ is the white noise that represents the atmosphere forcing, and σ_ξ^2 is the variance of this white noise. All the numerical results are from the last 500 years of a 1000-yr run. The numerical model Eqs. (2.1) and (2.2) are solved in the time step of 4 h.

We also perform ensemble forecasts in the ROM to compare the persistence with the prediction skill in the perfect model framework. We use each control run (it is used to calculate persistence) as the “truth.” For each of the forecast ensemble members (20 members), a small random normal perturbation (zero mean and 0.1 times the standard deviation of T) is added to variable T as the initial condition (Wang et al. 2021). We do ensemble forecasts in every month of 500 years with 12 months forecast length to get sufficient forecast data.

To derive the prediction skill of T in the ROM, two rules can be derived according to Eqs. (2.1) and (2.2). First, the variance of T is equal to the variance of H ; that is, $\langle T(t), T(t) \rangle = \langle H(t), H(t) \rangle$. Second, the covariance of T and H is zero; that is, $\langle T(t), H(t) \rangle = 0$. Note here that angle brackets denote the variance over all the months or years in verifying time series. Both rules are identified in the numerical solutions of the ROM (not shown).

b. The second-order autoregression model

The autoregression model has been used to study ENSO extensively (Torrence and Webster 1998; Ren et al. 2016; Liu et al. 2019). Note here that ROM needs both subsurface and surface information of tropical Pacific to perform ENSO retrospective forecasts [Eqs. (2.1) and (2.2)]. However, the subsurface dataset is not reliable before 1980. In this regard, we use the second-order autoregression (AR2) model to perform ENSO retrospective forecasts from 1910 to 2010 as ROM is one special form of an AR2 model. The relationship between these two models can be derived analytically (see the appendix for more details). The AR2 model that incorporates a seasonal cycle is as follows:

$$X_{i+1} = \alpha_m X_i + \beta_m X_{i-1} + N_{i+1}, \quad (2.3)$$

where X is the temperature anomaly, and subscript i is the time measured in months. The growth rates α_m and β_m are model parameters, which can be obtained by regressing X_{i+1} onto X_i , X_{i-1} respectively, where the subscript m is the seasonal cycle in months; N_{i+1} is random noise. When $\beta_m = 0$, the AR2 model is reduced to a first-order autoregression (AR1) model. The way we perform forecasts is same as what we do using ROM, except that we use observation as the “truth.”

c. Verification measure

In this study the forecast skill is verified using the ACC. ACC is defined as the temporal correlation coefficient between the ensemble mean forecast and the corresponding “truth”:

$$\text{ACC} = \frac{\langle F_i, O_i \rangle}{\sqrt{\langle F_i, F_i \rangle \langle O_i, O_i \rangle}}, \quad (2.4)$$

where F_i is the ensemble-mean forecast anomaly for forecast month or year i , and O_i is the verifying observed anomaly. The angle brackets denote the variance over all the months or years in verifying time series.

d. Data

Here we use the dataset from January 1910 to December 2010. The Hadley Centre Global Sea Ice and Sea Surface Temperature (HadISST; $1^\circ \times 1^\circ$) observational SST dataset version 1.1 (<https://climatedataguide.ucar.edu/climate-data/sst-data-hadisst-v11>) to define general features of the Niño-3.4 SST anomaly for ENSO. Monthly Niño-3.4 index anomalies are computed relative to the climatology of the corresponding running 20-yr window (Deng and Tang 2009), which could exclude the effects of low-frequency variations.

3. The relationship between persistence and prediction skill in ROM: Analytically and numerically

In this section, the ACC of T is solved both analytically and numerically in the finite difference of ROM [Eqs. (2.1) and (2.2)]. Accordingly, the relationship between persistence and predictability can be understood. For convenience of illustration,

we will derive the relation in the finite difference form of ROM, instead of the continuous form (e.g., Kleeman 2002). Furthermore, the seasonal cycle is not included in the analytical derivation.

a. The analytical solution of ACC in the ROM

The finite difference of Eqs. (2.1) and (2.2) can be written as follows:

$$T_{i+1} = aT_i + bH_i + \xi, \quad (3.1)$$

$$H_{i+1} = H_i - bT_i, \quad (3.2)$$

where $a = 1 - \lambda/\Delta t$, $b = \omega_0 \Delta t$, and Δt is the time step.

First, we should understand what a and b mean. According to Eq. (3.1), the two equations can be written as

$$\langle T_{i+1}, T_i \rangle = a \langle T_i, T_i \rangle + b \langle H_i, T_i \rangle \quad \text{and} \quad (3.3)$$

$$\langle T_{i+1}, H_i \rangle = a \langle T_i, H_i \rangle + b \langle H_i, H_i \rangle. \quad (3.4)$$

As mentioned above in section 2a, $\langle T_i, T_i \rangle = \langle H_i, H_i \rangle$ and $\langle T_i, H_i \rangle = 0$; according to Eq. (3.3), a can be derived as

$$a = \frac{\langle T_{i+1}, T_i \rangle}{\langle T_i, T_i \rangle} = \frac{\langle T_{i+1}, T_i \rangle}{\sqrt{\langle T_i, T_i \rangle \langle T_{i+1}, T_{i+1} \rangle}}. \quad (3.5)$$

It represents the lagged autocorrelation of T (i.e., persistence of T). Similarly, according to Eq. (3.4), b can be derived as

$$b = \frac{\langle T_{i+1}, H_i \rangle}{\langle H_i, H_i \rangle} = \frac{\langle T_{i+1}, H_i \rangle}{\sqrt{\langle H_i, H_i \rangle \langle T_{i+1}, T_{i+1} \rangle}}. \quad (3.6)$$

It represents the lagged cross correlation between H and T (H leads T). Note here b is also the parameter of ENSO linear periodicity; that is, a larger b represents a shortened ENSO period and a higher cross correlation at the early lead times (e.g., one time step).

We then link a and b with the ACC in the framework of perfect model forecasting. According to Eq. (3.1), when the ensemble number is infinite [as in Jin et al. (2018)], the ensemble mean of the forecast at the next time step (\overline{T}_{i+1}^f) can be written as

$$\overline{T}_{i+1}^f = aT_i + bH_i. \quad (3.7)$$

As such, the ACC of the forecast at the next step can be derived as

$$\begin{aligned} \text{ACC}_{i+1} &= \frac{\langle \overline{T}_{i+1}^f, T_{i+1} \rangle}{\sqrt{\langle \overline{T}_{i+1}^f, \overline{T}_{i+1}^f \rangle \langle T_{i+1}, T_{i+1} \rangle}} \\ &= \frac{\langle aT_i + bH_i, aT_i + bH_i + \xi \rangle}{\sqrt{\langle aT_i + bH_i, aT_i + bH_i \rangle \langle T_{i+1}, T_{i+1} \rangle}} = \sqrt{a^2 + b^2}. \end{aligned} \quad (3.8)$$

According to Eq. (3.8), the prediction skill of T is related to the persistence of T and the cross correlation between H and T .

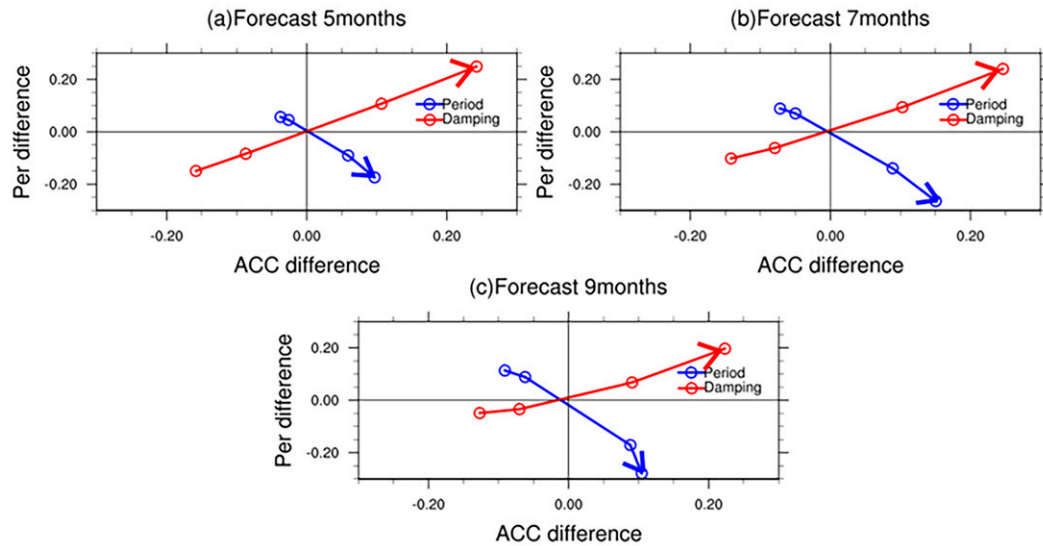


FIG. 2. The persistence and ACC relationship for different damping rates and ENSO periods. (a) The relationship at 5 months' forecast length. The red arrow indicates that the damping rate ranges from 0.25 to 0.05 month⁻¹ (red circle). The difference is calculated relative to the case when the damping rate is 0.15 month⁻¹ and the ENSO period is 4 years. The blue symbols are same as the red ones, except that the blue arrow indicates that the ENSO period ranges from 5 to 2.5 years. (b),(c) As in (a), but for forecast lengths of 7 and 9 months, respectively.

When b tends to be zero, the recharge oscillator model is reduced to the AR1 model, and the prediction skill is equal to the persistence of T , which is the persistence–skill rule identified in Jin et al. (2018). According to Eq. (3.8), a higher persistence (i.e., a larger a) can be related to a higher ACC when b is constant. However, when a lower persistence occurs (i.e., a is small), the prediction skill may not be lower if b is larger (a larger cross correlation between H and T).

b. The numerical solution of ACC in the ROM

In this subsection, we will show the relationship between persistence and ACC numerically as a confirmation of the analytical solution of Eq. (3.8).

The positive relationship between persistence and ACC occurs when the damping rate [λ in Eq. (2.1)] modulates. When $\lambda = 0.1$ month⁻¹, the persistence decays from 1 to 0.4 after about 6 months (black dashed line in Fig. 1a). The ACC of this case (more details about forecasting can be checked in section 2a) is still about 0.6 when forecast length is 10 months (black solid line in Fig. 1a). The difference between persistence and ACC is caused by the information provided by the subsurface. When the damping rate is increased to 0.2 month⁻¹ (the system is more damping), the persistence decays to 0.4 after 4 months (red dashed line in Fig. 1a), which is shorter than the previous case. This is straightforward to understand as the system damps more quickly. Meanwhile, ACC decays to about 0.4 after 10 months (red solid line in Fig. 1a), which is also lower than the previous case. This is consistent with the persistence–skill rule (Jin et al. 2018); when the persistence of “truth” is lower, the prediction skill tends to be smaller. This relationship is also indicated by Eq. (3.8).

This positive relationship between persistence and ACC turns out to be negative when the ENSO period changes [ω_0 in Eq. (2.1), which can be employed to control the cross correlation between H and T]. When ENSO's linear period is 4 years [$\omega_0 = (\pi/24)$ month⁻¹], the persistence is 0.4 at 6 months lead time (black dashed line in Fig. 1b). The ACC of this case at the same lead time is 0.6, which is higher than persistence (black solid vs dashed line in Fig. 1b). For the case when the ENSO period is 2.5 years [$\omega_0 = (\pi/24)$ month⁻¹], the persistence is lower than the case of 4 years (red dashed line vs black dashed line in Fig. 1b), on the other hand, ACC is about 0.7 when forecast length is 6 months, which is higher. A lower persistence is accompanied with a higher ACC, which is also suggested in Eq. (3.8). Note here that when damping rate increases from 0.1 to 0.15 month⁻¹, this effect of prediction will be cancelled out roughly when ENSO period decreases from 4 to 3 years.

The different relationships between persistence and ACC are further identified in Fig. 2. For a forecast length of 5 months, when the damping rate linearly decreases from 0.25 to 0.05 month⁻¹, the persistence increases and so does the ACC. The red line in Fig. 2a indicates this positive relationship between persistence and ACC. However, when ENSO's period is shortened from 5 to 2.5 years, the persistence is decreased while ACC is increased (blue line in Fig. 2a). The blue line shows a distinct negative relationship between persistence and ACC, which is opposite to the damping rate cases. The situation is similar when forecast month is lengthened (Figs. 2b,c).

In this section, we demonstrate that the predictability comes from the persistence and the cross correlation with the subsurface in the framework of the recharge oscillator. We demonstrate analytically and numerically that although the

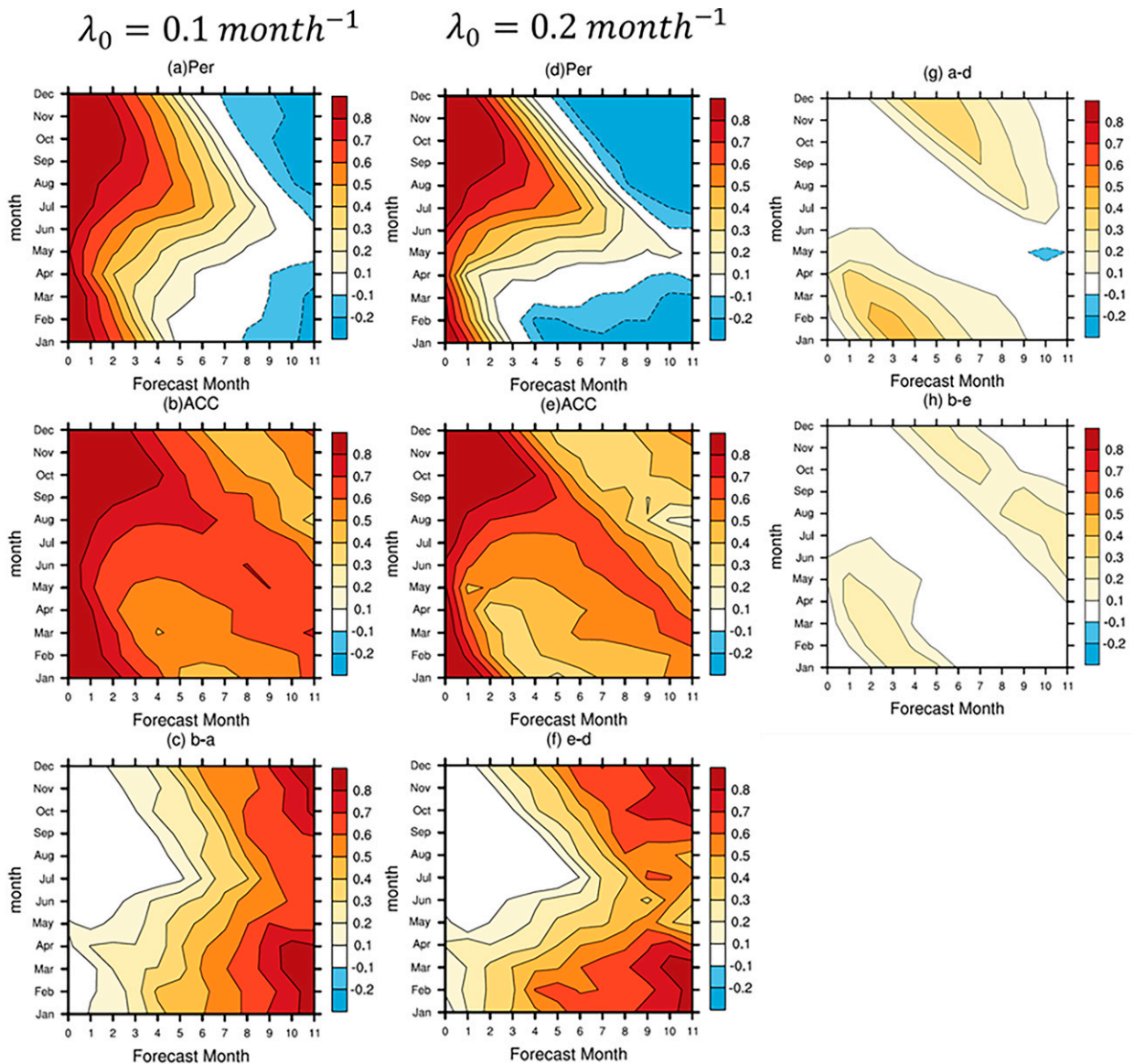


FIG. 3. The persistence and ACC map relationship for different damping rates. ENSO period is 4 years (constant). (a),(b) The persistence map and ACC map, respectively, when $\lambda_0 = 0.1 \text{ month}^{-1}$. (c) The difference (b) – (a). (d)–(f) As in (a)–(c), respectively, except when $\lambda_0 = 0.2 \text{ month}^{-1}$. (g) The difference (a) – (d). (h) The difference (b) – (e).

persistence is lower, the final prediction skill may be higher because of the subsurface (i.e., OHC). Particularly, in damping rate cases, a stronger PB is identical to a stronger PD. However, when the ENSO period varies, a stronger PB is accompanied with a weaker PD. As such, a stronger PB may not indicate a stronger PD, which is further discussed in section 4.

4. The relationship between spring PB and PD in the seasonally varying ROM

We first discuss the relationship between spring PB and PD when the damping rate changes. Note that seasonal cycle of the damping rate (λ) is the cause of spring PB (Levine and

McPhaden 2015). Here we set $\lambda(t) = \lambda_0 [1 + A \sin(\omega_A t)]$, with $\omega_A = (2\pi/12) \text{ month}^{-1}$ as the annual frequency and $A = 1.7 \text{ month}^{-1}$ (Jin et al. 2021). Previous studies have shown that annual mean damping rate (i.e., λ_0) plays an important role in spring PB strength (Liu et al. 2019; Jin et al. 2020). As such, we vary λ_0 to see the relationship between spring PB and PD. When $\lambda_0 = 0.1 \text{ month}^{-1}$, a distinct spring PB can be seen in Fig. 3a. Meanwhile, the ACC map shows a clear spring PD (Fig. 3b). The major difference between the ACC map and the persistence map is the higher prediction skill at the longer lead time for ACC (Fig. 3c). A strong cross-correlation between the surface and subsurface at longer lead times may help improve the prediction skill (Jin et al. 2021), especially

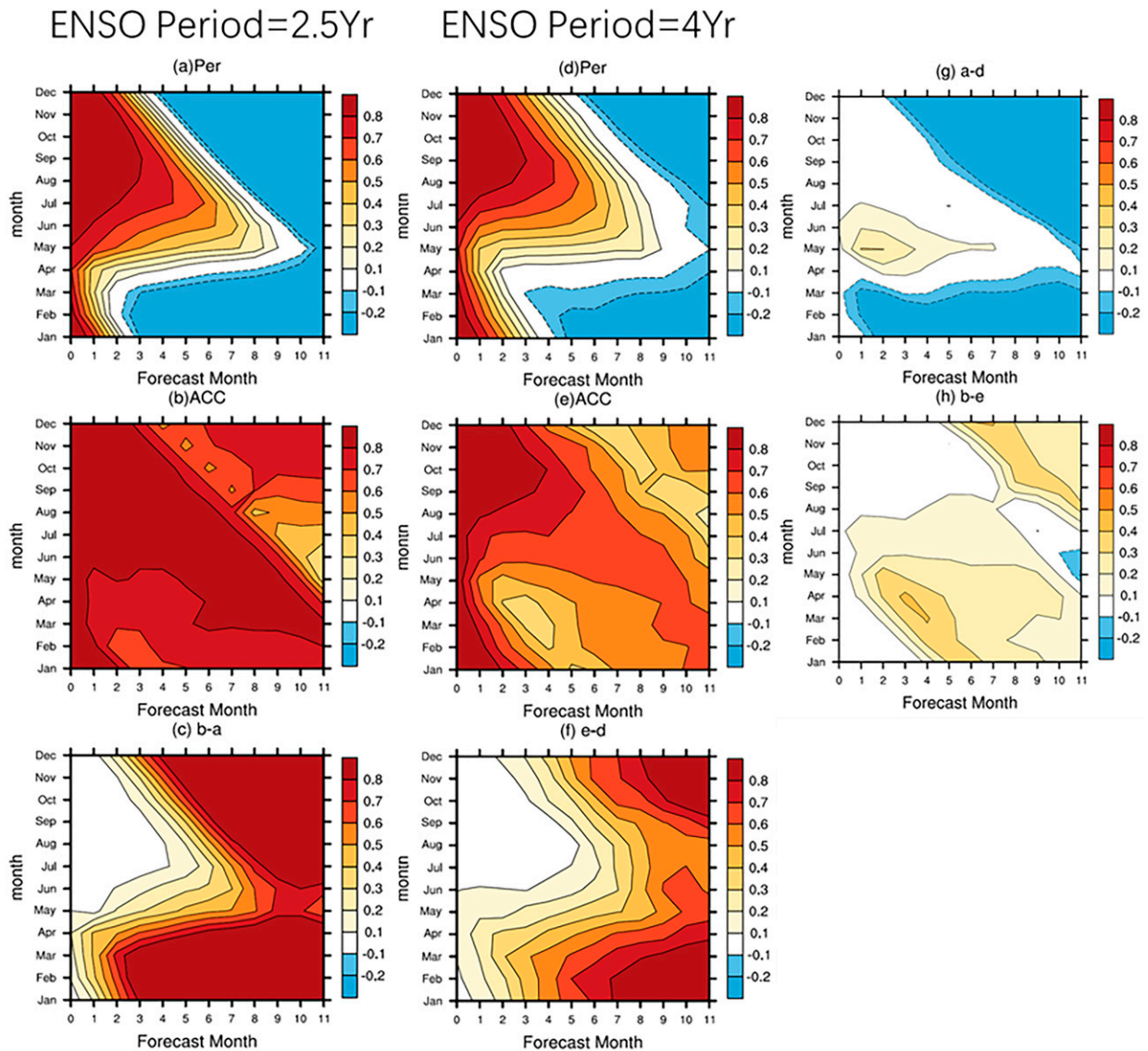


FIG. 4. The persistence and ACC map relationship for different ENSO periods; $\lambda_0 = 0.15 \text{ month}^{-1}$ (constant). (a),(b) The persistence map and ACC map, respectively, when the ENSO period is 2.5 years. (c) The difference (b) – (a). (d)–(f) As in (a)–(c), respectively, but when the ENSO period is 4 years. (g) The difference (a) – (d). (h) The difference (b) – (e).

when the initial month is in spring. The additional information from the subsurface helps across the spring PD, which is consistent with McPhaden (2003). When we further increase λ_0 to 0.2 month^{-1} such that the system is more damping, a stronger spring PB associated with a stronger spring PD (Figs. 3d,e) can be found. A similar role of the subsurface in ENSO prediction can be seen in Fig. 3f, which is consistent with Fig. 3c. The role of λ_0 in ENSO spring PB and PD can be further checked in Figs. 3g and 3h. When we increase λ_0 , a stronger spring PB (Fig. 3g) and spring PD (Fig. 3h) are found, which suggests a positive relationship: a stronger spring PB is accompanied with a stronger spring PD. This is consistent with Fig. 1a (or red line in Fig. 2).

This positive relationship between spring PB and PD turns out to be negative when the ENSO period varies. When ENSO's linear period is 2.5 years [$\omega_0 = (\pi/24) \text{ month}^{-1}$], a very strong spring PB and low persistence (e.g., at about 8 months' lead time) can be found in Fig. 4a. However, a weak spring PD is associated with higher prediction skill at the same lead time (Fig. 4b). The major difference between the ACC and persistence maps is in the large lead time (Fig. 4c). The subsurface information strongly increases ACC because of this short ENSO period. In particular, a strong cross-correlation between the surface and subsurface of the tropical Pacific can help increase ACC (e.g., 6 months' lead time), which is controlled by the ENSO period. For

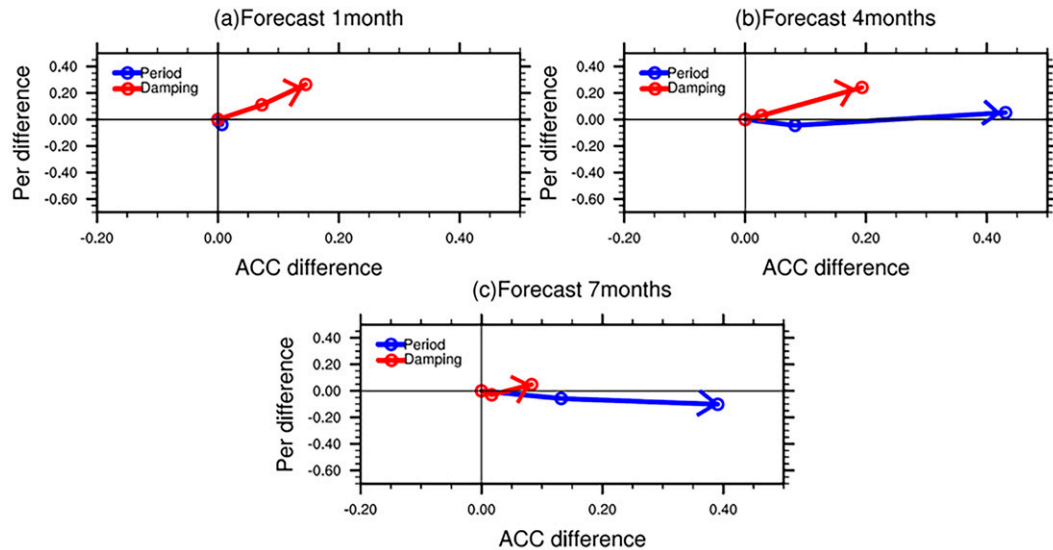


FIG. 5. As in Fig. 2, but the initial season is spring (averaged from March to May). (a) The relationship at 1 month forecast length. The red arrow indicates that damping rate ranges from 0.3 to 0.1 month⁻¹ (red circles). The difference is calculated relative to the case when damping rate is 0.3 month⁻¹ and ENSO period is 4 years. The blue symbols are the same as the red ones, except that the ENSO period ranges from 5 to 2.5 years and the difference is calculated relative to the case when the damping rate is 0.15 month⁻¹ and ENSO period is 5 years. (b),(c) As in (a), but for forecast lengths of 4 and 7 months, respectively.

$\omega_0 = (\pi/24)$ month⁻¹ (when the ENSO period is 4 years), a much weaker spring PB (Fig. 4d) occurs compared with a shortened ENSO period. On the other hand, the ACC map (Fig. 4e) indicates that a relatively stronger PD compared with Fig. 4b. This point can also be identified in Figs. 4g and 4h. When the ENSO period decreases from 4 to 2.5 years, persistence map shows a clearly stronger PB (Fig. 4g) while the ACC map indicates a weaker spring PD (Fig. 4h). This can be understood using Eq. (3.8). Although the persistence is lower, the information from the subsurface also supports a larger ACC. Note here that in addition to the strength of the PB and PD, Fig. 4 also suggests that PB is shifted a month earlier for the 2.5-yr period compared to the 4-yr period. By using the analytical solution of ROM, Jin and Liu (2021) [their Eqs. (3.11) and (3.12)] demonstrates that a shortened ENSO period is accompanied with an earlier timing of PB.

The different relationships between spring PB and PD can be further identified in Fig. 5. At the first month lead time, a weaker PB is associated with a weaker PD, which can be found in the damping cases (λ_0 is decreased from 0.3 to 0.1 month⁻¹) when the initial season is in the spring (red circles in Fig. 5a). When lead time increases to 4 or 7 months, this positive relationship can still be identified (red circles in Figs. 5b,c). This is consistent with Fig. 3 when we vary damping rates. Meanwhile, at 4 months' lead time, a smaller PD can be found for the period cases (the ENSO period decreases from 5 to 2.5 years) when the initial month is in the spring. When lead time increases to 4 or 7 months, a stronger PB accompanied with a smaller PD can be found (blue circles in Fig. 5c), which is consistent with Fig. 4 when we vary ENSO periods. Here for damping cases, we use 4 years as the

baseline because generally the ENSO period is 4 years. In ENSO period cases, we use 5 years as the baseline such that the difference of ACC or persistence can be in the same direction when we range the ENSO period from 5 to 2.5 years.

In this section, we show that a stronger PB may not always correspond to a stronger PD. The information from the subsurface can also lead to a higher predictability such that a weaker PD occurs when the persistence map shows a stronger PB.

5. The explanation of interdecadal modulation of ENSO prediction skill in the observations

In this section, we will explain the interdecadal modulation of ENSO prediction skill in the observations in light of our analytical and numerical solutions in the ROM.

ENSO prediction skill exhibits interdecadal modulation. Forecast skill is evaluated retrospectively by using Eq. (2.3). Retrospective forecasts start at every month from January 1910 to January 2010 (more details can be seen in section 2) with a 20-yr moving window. The ACC exhibits a distinct interdecadal modulation (red line in Fig. 6a), with one significant feature being the higher ACC after about 1960, which is similar to Weisheimer et al. (2020, their Fig. 4c) or Weisheimer et al. (2022) and to Liu et al. (2021; blue or red line in their Fig. 5) through the coupled general circulation models forecasting. This feature also exists when the forecast length is 8 months (red line in Fig. 6b). Here it exhibits some differences in ACC at different forecast lead times that may be caused by the role of the subsurface. The role of the subsurface in forecasting is different at different lead times (Jin et al. 2021). The large difference between persistence and predictability occurs after

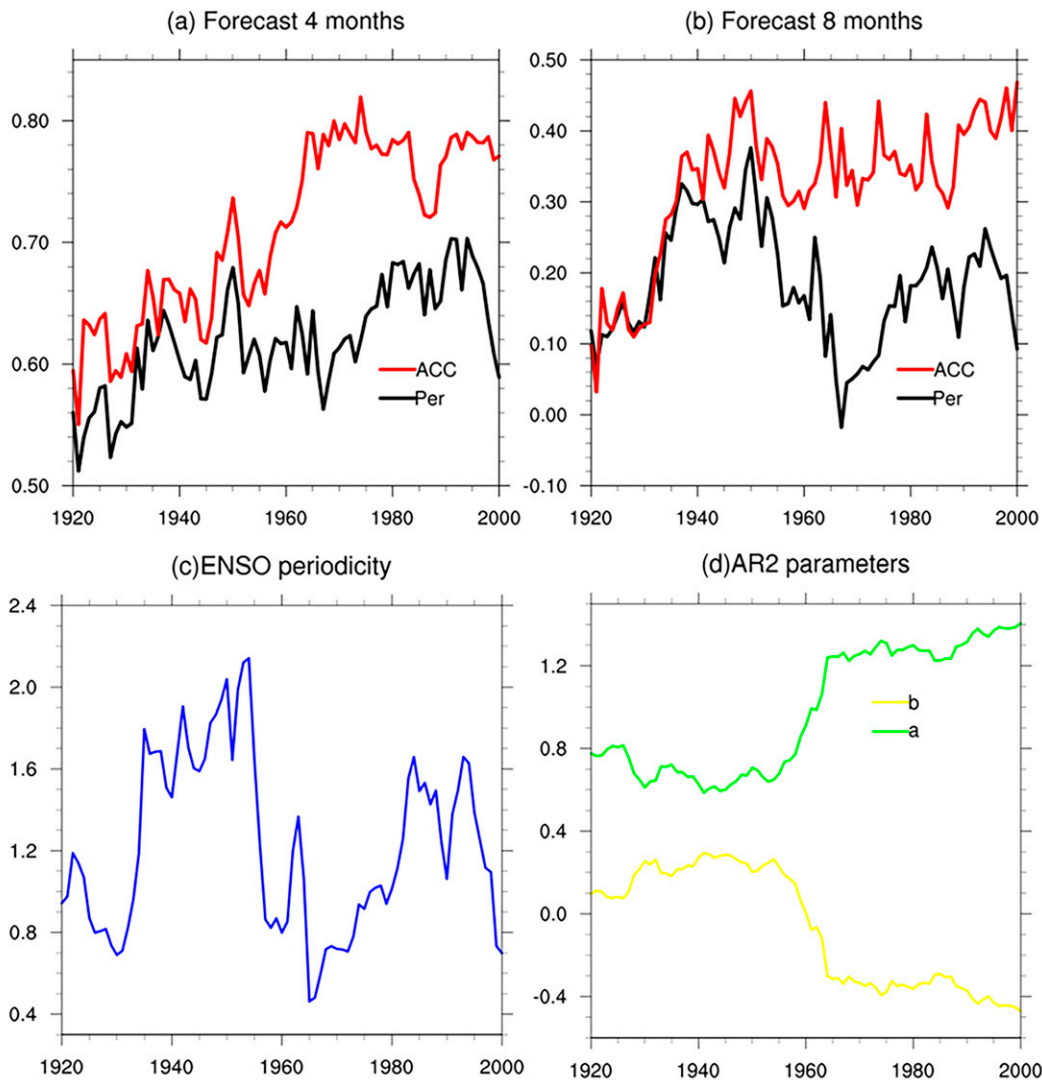


FIG. 6. The persistence (black) and ACC (red) for ENSO from 1910 to 2010 with 20-yr moving window at (a) 4 and (b) 8 months' forecast length, respectively. (c) ENSO periodicity is calculated as the ratio between ENSO SST spectral energy in the 3–8-yr band and that in the 1–3-yr band, as in Lu et al. (2018). (d) The interdecadal variation of AR2 model parameters [α : green line; β : yellow line in Eq. (2.3)] fitted by observations.

1960, which may be caused by the interdecadal modulation of the system. According to our analytical solution of ACC [Eq. (3.8)], this difference is caused by the lead relationship between the subsurface and surface in the tropical Pacific. Previous studies have shown that this lead relationship is related to the ENSO period (Jin et al. 2021). A shortened ENSO period will lead to a larger lead relationship and a higher ACC at the lead times. As such, the ENSO period may play a role in the difference between persistence and ACC. Figure 6c demonstrates the ENSO period modulation during 1910–2010. It is suggested that the ENSO period is shortened after 1960, which is consistent with the timing of a higher ACC. Accordingly, we suggest that a shortened ENSO period is a key cause for a higher ENSO ACC after 1960. Note here that a stronger thermocline feedback may

cause a shortened ENSO period (Jin 1997), and the relationship between the multidecadal variation of ENSO prediction skill and thermocline feedback requires further study. It should be pointed out that a lower prediction skill around 1920 is also accompanied by the shortened period. It may be related to the stronger damping of the system (green line in Fig. 6d; Deng and Tang 2009).

We also demonstrate that including subsurface information may lead to a weaker spring PD (McPhaden 2003). A strong spring PB occurs during the year 1980–2010 (Fig. 7a). Through the retrospective forecasts using AR2 model, a spring PD is also found (Fig. 7b). This explains that a spring PB is always associated with a PD. However, a higher ACC is found at the large lead time (about 5–10 months) when the initial month is in the spring, which suggests the role of the subsurface. This

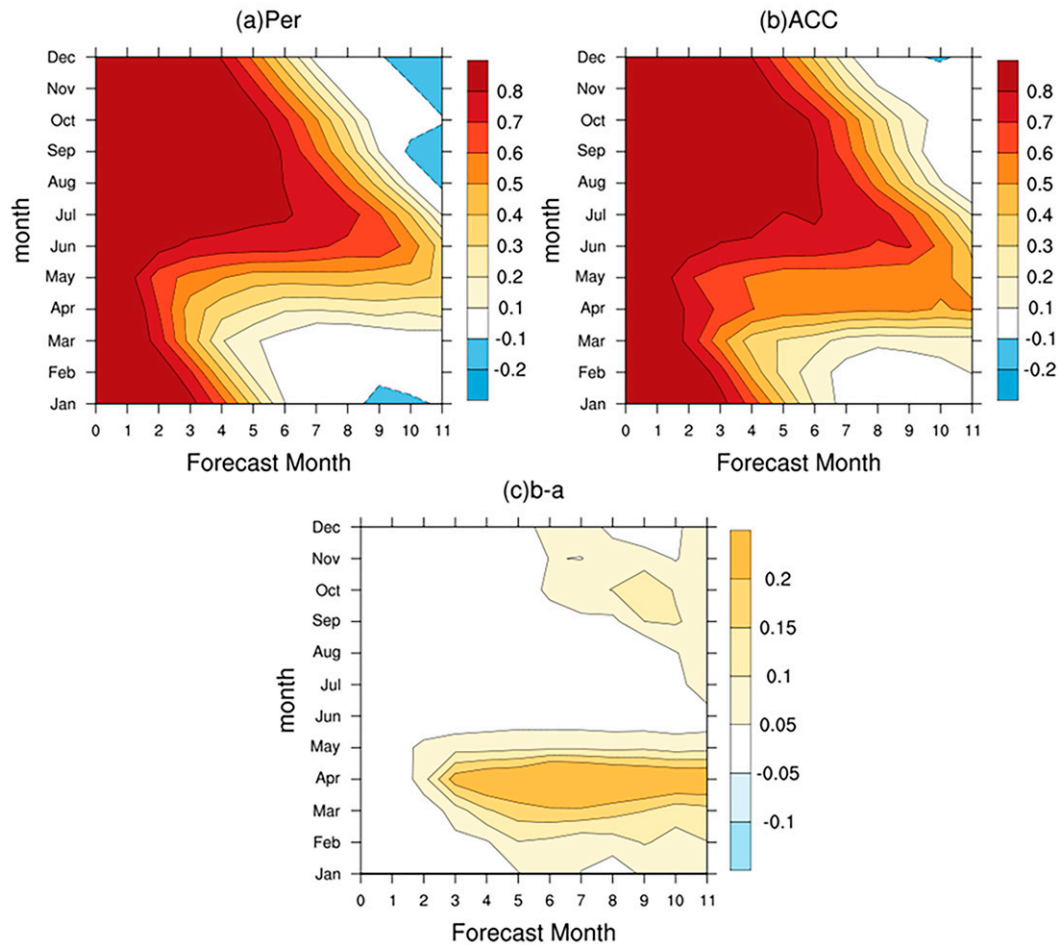


FIG. 7. The (a) persistence map and (b) ACC map using 1980–2010 data. (c) The difference (b) – (a).

point can be further identified in Fig. 7c. It is demonstrated that the main role of the subsurface is in the spring, which weakens the PD. As such, a strong PB may not correspond to a strong PD as the existence of the subsurface ocean heat content.

The role of the subsurface in significantly reducing spring PD occurs after 1960, which is related to the interdecadal modulation of ENSO period. Before 1960, the difference between persistence and ACC is small for different initial seasons (black line vs red line, and blue line vs brown line in Fig. 8a) at 4 months' lead time. After 1960, although the persistence and ACC also exhibit small differences when the initial season is autumn, they show a distinct difference when the initial season is spring. The situation is similar when lead time is lengthened (Fig. 8b). Here we suggest that it is caused by the interdecadal modulation of the ENSO period. When the ENSO period is longer (before 1960; Fig. 6c), the cross correlation is small at the short lead time (Jin et al. 2021). As such, ACC is close to the persistence, which is according to our analytical solution [Eq. (3.8)]. When the ENSO period is shortened (after 1960), the cross correlation is large and ACC is higher than persistence. As the subsurface information plays

a main role in the spring, which is shown in Fig. 7c, the large difference between ACC and persistence can be seen when the initial season is spring (red line vs black line in Figs. 8a,b).

6. Summary and discussion

This paper attempts to understand the relationship between ENSO's spring persistence barrier and predictability barrier both analytically and numerically and apply it to explain the interdecadal modulation of ENSO prediction skill. The relationship between ACC and persistence is obtained in the framework of the recharge oscillator. According to the analytical solution of SST ACC, it is suggested that ACC is the sum of persistence and cross correlation between SST and the subsurface in the tropical Pacific. Unlike the persistence–skill rule identified by Jin et al. (2018) using an AR1 model, which suggests that large persistence will cause a high ACC, this theory indicates the role of the subsurface. Both analytical and numerical solution demonstrate that a small growth rate (or a large damping rate) will lead to a low persistence and small predictability; on the other hand, a shortened ENSO period will cause a small persistence and a large cross correlation,

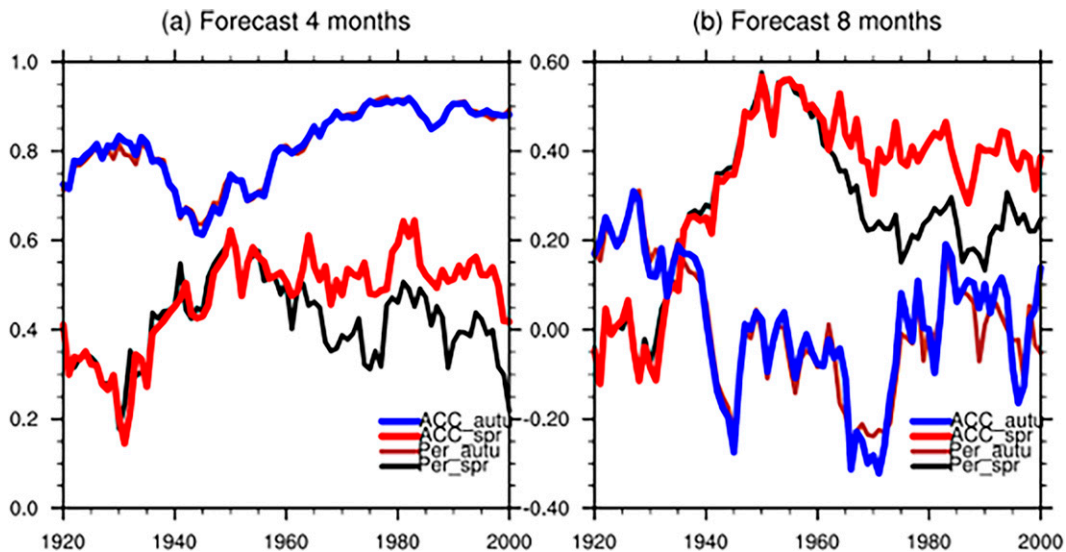


FIG. 8. (a) The persistence and ACC for ENSO from 1910 to 2010 with 20-yr moving window at 4 months; the black and red lines are persistence and ACC respectively when the initial month is in the spring; the brown and blue lines are the same as the black and red lines, respectively, except the initial season is in the autumn. (b) As in (a), but for the forecast length is 8 months.

and thus the final predictability is not low. Accordingly, persistence is not identical to predictability and the spring persistence barrier may also not be identical to the spring predictability barrier. Further numerical solutions show that when the growth rate is smaller, a stronger persistence barrier associated with a stronger predictability barrier is found. When the ENSO period is shortened, a stronger persistence barrier accompanied with a weaker predictability barrier is identified. We then apply our theory to explain the interdecadal modulation of ENSO prediction skill. A larger difference between persistence and ACC is found after 1960, especially when the initial month is spring. It is suggested that this large difference may be related to the shortened ENSO period after 1960. A shortened ENSO period can lead to a stronger cross-correlation between the surface and subsurface of the tropical Pacific (Jin et al. 2021), which can help increase ACC at different lead times (e.g., 6 months).

Our solution may give an example to explain the interdecadal modulation of ENSO prediction skill with the climate system. It should be noted here other factors like data assimilation or the quality of observation data are of great importance in ENSO prediction. Here we give another view using the modulation of climate system in the tropical Pacific. It is consistent with Weisheimer et al. (2020), who also found that the interdecadal modulation of ENSO prediction skill may related to intrinsic changes of the coupled system. Our solutions suggest the role of ENSO period, but what causes the interdecadal modulation of ENSO period after 1960 still needs further study.

ENSO variability (or amplitude) can also play an important role in ENSO prediction. Generally, a larger SST intensity (or ENSO amplitude) may correspond to a higher prediction skill (e.g., Jin et al. 2008; see their Fig. 11c). A stronger growth of the ENSO signal can lead to a larger ENSO amplitude and,

accordingly, higher prediction skill. In fact, this can be identified through the analytical solutions of the ROM [Eqs. (2.1) and (2.2)]. By using the perturbation method (Jin et al. 2021; their appendix B), the variance of T (i.e., ENSO variability) can be derived analytically (not shown). It is found that the variance of T is only related to damping rate and forcing variance (or noise variance) instead of ENSO linear frequency. When the damping rate is smaller (i.e., the growth rate is larger), ENSO variability is larger and the prediction skill is higher according to the analytical/numerical solutions in this paper. This may explain the relationship between ENSO variability and prediction skill. On the other hand, ENSO linear frequency has no relationship with variability. Note here that white noise forcing plays a less important role in ENSO prediction [Eq. (3.8)]; it can also be identified in Liu et al. (2019)]. Therefore, the discussion of the relationship between noise forcing and ENSO amplitude is beyond the scope of this paper.

Note that our result of the relationship between persistence barrier and predictability barrier in a simple model is similar to previous studies using the fully coupled models (Hou et al. 2019). Duan and Hu (2015) suggested that a predictability barrier occurs when the ENSO-associated SST anomalies yield a persistence barrier. In other words, only a specific type of persistence barrier can lead to a predictability barrier. Here we suggest that this relationship can be influenced by the information from the subsurface of the tropical Pacific.

Our solution does not indicate that the persistence–skill rule pointed out by Jin et al. (2018) is wrong. The persistence–skill rule is derived in the AR1 model, which represents a system that is purely damping (i.e., no periodicity). Many areas like the North Pacific exhibit this process (Liu et al. 2019). Our solution here is obtained as ENSO has its own frequency and may give some implications for other periodic climate systems

(e.g., Pacific decadal oscillation). When the ENSO period tends to be infinitely long, our solutions are reduced to the persistence–skill rule.

Determining what causes lower ENSO prediction skill after the twenty-first century may require deep thought. According to Jin et al. (2021), the shortened ENSO period leads to a stronger spring persistence barrier and thus may cause a lower prediction skill after the twenty-first century through the ROM. However, our solutions here find that a shortened ENSO period may lead to a higher prediction skill at the early lead times (e.g., less than 12 months) and a weaker spring predictability barrier. Accordingly, the stronger damping system of tropical Pacific after twenty-first century may be a reason for lower ENSO prediction skill (Jin et al. 2020).

We should also bear in mind that other climate systems may also affect the predictability and predictability barrier of ENSO. Our solution is derived in the recharge oscillator framework. Many other factors may also contribute to ENSO development and thus its predictability. For example, the northern meridional mode may be an important role in triggering ENSO in the spring and may reduce the spring predictability barrier (Chang et al. 2007). How to consider these effects still needs further work.

Acknowledgments. The authors thank the editor and two anonymous reviewers for their helpful comments on this study. This work is supported by Shandong Provincial Natural Science Foundation, China, ZR202102240275.

Data availability statement. HadISST v1.1 data can be downloaded online at <https://climatedataguide.ucar.edu/climate-data/sst-data-hadisst-v11>.

APPENDIX

The Relationship Between the AR2 Model and Recharge Oscillator

According to the finite difference of Eqs. (3.1) and (3.2), the recharge oscillator can be written as

$$T_{i+1} = aT_i + bH_i + \xi, \quad (\text{A.1})$$

$$H_{i+1} = H_i - bT_i. \quad (\text{A.2})$$

Taking Eq. (A.2) to Eq. (A.1), we can obtain

$$T_{i+1} = aT_i + b(H_{i-1} - bT_{i-1}) + \xi_1. \quad (\text{A.3})$$

Meanwhile, T_i can be written as

$$T_i = aT_{i-1} + bH_{i-1} + \xi_2. \quad (\text{A.4})$$

To eliminate H , taking Eq. (A.4) to Eq. (A.3),

$$T_{i+1} = \alpha T_i + \beta T_{i-1} + \zeta, \quad (\text{A.5})$$

where $\alpha = (1 + a)$, $\beta = -(a + b^2)$, and ζ is the noise term. Equation (A.5) suggests that the recharge oscillator is one special form of AR2 model.

REFERENCES

- Anderson, B. T., 2007: On the joint role of subtropical atmospheric variability and equatorial subsurface heat content anomalies in initiating the onset of ENSO events. *J. Climate*, **20**, 1593–1599, <https://doi.org/10.1175/JCLI4075.1>.
- Burgers, G., F.-F. Jin, and G. J. van Oldenborgh, 2005: The simplest ENSO recharge oscillator. *Geophys. Res. Lett.*, **32**, L13706, <https://doi.org/10.1029/2005GL022951>.
- Cai, W., and Coauthors, 2018: Increased variability of eastern Pacific El Niño under greenhouse warming. *Nature*, **564**, 201–206, <https://doi.org/10.1038/s41586-018-0776-9>.
- Chang, P., L. Zhang, R. Saravanan, D. J. Vimont, J. C. H. Chiang, L. Ji, H. Seidel, and M. K. Tippett, 2007: Pacific meridional mode and El Niño–Southern Oscillation. *Geophys. Res. Lett.*, **34**, L16608, <https://doi.org/10.1029/2007GL030302>.
- Deng, Z., and Y. Tang, 2009: The retrospective prediction of ENSO from 1881 to 2000 by a hybrid coupled model: (II) Interdecadal and decadal variations in predictability. *Climate Dyn.*, **32**, 415–428, <https://doi.org/10.1007/s00382-008-0398-2>.
- Duan, W., and J. Hu, 2015: The initial errors that induce a significant “spring predictability barrier” for El Niño events and their implications for target observation: Results from an Earth system model. *Climate Dyn.*, **46**, 3599–3615, <https://doi.org/10.1007/s00382-015-2789-5>.
- Hou, M., W. Duan, and X. Zhi, 2019: Season-dependent predictability barrier for two types of El Niño revealed by an approach to data analysis for predictability. *Climate Dyn.*, **53**, 5561–5581, <https://doi.org/10.1007/s00382-019-04888-w>.
- Jin, E. K., and Coauthors, 2008: Current status of ENSO prediction skill in coupled ocean–atmosphere models. *Climate Dyn.*, **31**, 647–664, <https://doi.org/10.1007/s00382-008-0397-3>.
- Jin, F.-F., 1997: An equatorial ocean recharge paradigm for ENSO. Part I: Conceptual model. *J. Atmos. Sci.*, **54**, 811–829, [https://doi.org/10.1175/1520-0469\(1997\)054<0811:AEORPF>2.CO;2](https://doi.org/10.1175/1520-0469(1997)054<0811:AEORPF>2.CO;2).
- Jin, Y., and Z. Liu, 2021: A theory of the spring persistence barrier on ENSO. Part I: The role of ENSO period. *J. Climate*, **34**, 2145–2155, <https://doi.org/10.1175/JCLI-D-20-0540.1>.
- , X. Rong, and Z. Liu, 2018: Potential predictability and forecast skill in ensemble climate forecast: A skill-persistence rule. *Climate Dyn.*, **51**, 2725–2742, <https://doi.org/10.1007/s00382-017-4040-z>.
- , Z. Lu, and Z. Liu, 2020: Controls of spring persistence barrier strength in different ENSO regimes and implications for 21st century changes. *Geophys. Res. Lett.*, **47**, e2020GL088010, <https://doi.org/10.1029/2020GL088010>.
- , Z. Liu, and M. J. McPhaden, 2021: A theory of the spring persistence barrier on ENSO. Part III: The role of tropical Pacific Ocean heat content. *J. Climate*, **34**, 8567–8577, <https://doi.org/10.1175/JCLI-D-21-0070.1>.
- Kleeman, R., 2002: Measuring dynamical prediction utility using relative entropy. *J. Atmos. Sci.*, **59**, 2057–2072, [https://doi.org/10.1175/1520-0469\(2002\)059<2057:MDPUUR>2.0.CO;2](https://doi.org/10.1175/1520-0469(2002)059<2057:MDPUUR>2.0.CO;2).
- Levine, A. F. Z., and M. J. McPhaden, 2015: The annual cycle in ENSO growth rate as a cause of the spring predictability barrier. *Geophys. Res. Lett.*, **42**, 5034–5041, <https://doi.org/10.1002/2015GL064309>.
- Liu, T., X. Song, Y. Tang, Z. Shen, and X. Tan, 2021: ENSO predictability over the past 137 years based on a CESM ensemble prediction system. *J. Climate*, **35**, 763–777, <https://doi.org/10.1175/JCLI-D-21-0450.1>.

- Liu, Z., Y. Jin, and X. Rong, 2019: A theory for the seasonal predictability barrier: Threshold, timing, and intensity. *J. Climate*, **32**, 423–443, <https://doi.org/10.1175/JCLI-D-18-0383.1>.
- Lorenz, E. N., 1963: Deterministic nonperiodic flow. *J. Atmos. Sci.*, **20**, 130–141, [https://doi.org/10.1175/1520-0469\(1963\)020<0130:DNF>2.0.CO;2](https://doi.org/10.1175/1520-0469(1963)020<0130:DNF>2.0.CO;2).
- Lu, B., F.-F. Jin, and H.-L. Ren, 2018: A coupled dynamic index for ENSO periodicity. *J. Climate*, **31**, 2361–2376, <https://doi.org/10.1175/JCLI-D-17-0466.1>.
- McPhaden, M. J., 2003: Tropical Pacific Ocean heat content variations and ENSO persistence barriers. *Geophys. Res. Lett.*, **30**, 1480, <https://doi.org/10.1029/2003GL016872>.
- , S. E. Zebiak, and M. H. Glantz, 2006: ENSO as an integrating concept in Earth science. *Science*, **314**, 1740–1745, <https://doi.org/10.1126/science.1132588>.
- Meinen, C. S., and M. J. McPhaden, 2000: Observations of warm water volume changes in the equatorial Pacific and their relationship to El Niño and La Niña. *J. Climate*, **13**, 3551–3559, [https://doi.org/10.1175/1520-0442\(2000\)013<3551:OOWWVC>2.0.CO;2](https://doi.org/10.1175/1520-0442(2000)013<3551:OOWWVC>2.0.CO;2).
- Ren, H. L., F.-F. Jin, B. Tian, and A. A. Scaife, 2016: Distinct persistence barriers in two types of ENSO. *Geophys. Res. Lett.*, **43**, 10 973–10 979, <https://doi.org/10.1002/2016GL071015>.
- Torrence, C., and P. J. Webster, 1998: The annual cycle of persistence in the El Niño/Southern Oscillation. *Quart. J. Roy. Meteor. Soc.*, **124**, 1985–2004, <https://doi.org/10.1002/qj.49712455010>.
- Troup, A., 1965: The ‘southern oscillation.’ *Quart. J. Roy. Meteor. Soc.*, **91**, 490–506, <https://doi.org/10.1002/qj.49709139009>.
- Walker, G. T., and E. W. Bliss, 1932: World weather V. *Mem. Roy. Meteor. Soc.*, **4**, 53–84.
- Wang, P., Y. Jin, and Z. Liu, 2021: A diurnal predictability barrier for weather forecasts. *Mon. Wea. Rev.*, **149**, 1715–1723, <https://doi.org/10.1175/MWR-D-20-0205.1>.
- Webster, P. J., and S. Yang, 1992: Monsoon and ENSO: Selectively interactive systems. *Quart. J. Roy. Meteor. Soc.*, **118**, 877–926, <https://doi.org/10.1002/qj.49711850705>.
- Weisheimer, A., D. J. Bofort, D. MacLeod, T. Palmer, C. O’Reilly, and K. Strømme, 2020: Seasonal forecasts of the twentieth century. *Bull. Amer. Meteor. Soc.*, **101**, E1413–E1426, <https://doi.org/10.1175/BAMS-D-19-0019.1>.
- , M. A. Balmaseda, T. N. Stockdale, M. Mayer, S. Sharmila, H. Hendon, and O. Alves, 2022: Variability of ENSO forecast skill in 2-year global reforecasts over the 20th century. *Geophys. Res. Lett.*, **49**, e2022GL097885, <https://doi.org/10.1029/2022GL097885>.
- Wright, P. B., 1979: Persistence of rainfall anomalies in the central Pacific. *Nature*, **277**, 371–374, <https://doi.org/10.1038/277371a0>.